Theoretical study of pressure-driven phase transitions in HgSe and HgTe

S. Radescu, A. Mujica, and J. López-Solano
Departamento de Física Fundamental II, MALTA Consolíder Team, Universidad de La Laguna, La Laguna 38205, Tenerife, Spain

R. J. Needs
Cavendish Laboratory, University of Cambridge, 19 J.J. Thomson Avenue, Cambridge CB3 0HE, United Kingdom
(Received 21 September 2010; published 7 March 2011)

We present the results of a density-functional-theory study of the stability of high-pressure phases of HgSe and HgTe up to the so-called Cmcm phase, which is the highest-pressure phase that has been fully characterized in experiments in these compounds. We compare the results obtained using different exchange-correlation functionals for the energetics, stability, and structure of the high-pressure phases, finding that the qualitative picture is very similar and essentially in agreement with the experimental observations. We study the cinnabar → NaCl and the NaCl → Cmcm transitions in detail and provide the structural evolution under pressure of the cinnabar and Cmcm phases. We find that the mechanism for the NaCl → Cmcm transition is somewhat different from other related compounds exhibiting this transition, with cell deformation playing an important role in the stabilization of the Cmcm state in HgSe and HgTe. Our results support the view of a NaCl → Cmcm transition that is distinctly first order, in good agreement with the experimental observations and contrary to other materials where this transition is of second order.

DOI: 10.1103/PhysRevB.83.094107 PACS number(s): 64.60.Ej, 71.15.Nc, 62.50.−p, 63.20.−e

I. INTRODUCTION

The behavior under pressure of the mercury chalcogenides is probably the least theoretically studied within the II-VI family of compounds. Experimentally, the mercury chalcogenides HgSe and HgTe appear to adopt similar structures under compression.[1] Their ambient zincblende phases (which, unlike other group-II chalcogenides, are zero-gap semiconductors) transform into semiconducting phases with cinnabar-like structures at moderate pressures slightly above 1 GPa.[1–10] On further compression the cinnabar phases transform into the NaCl-type (rocksalt) structure at ∼15 GPa in HgSe (Refs. 1,6,7 and 11) and ∼8 GPa in HgTe.[1,6,7,11,12] A further transition takes place at higher pressures [∼28 GPa in HgSe (Refs. 11 and 13) and ∼10 GPa in HgTe (Refs. 11 and 12)] to a phase whose structure was first correctly characterized by McMahon *et al.*[14] This structure, named Cmcm after its space group, is an orthorhombic distortion of the NaCl structure that has also been observed in other members of the II-VI and III-V families of binary compounds,[1,15] and it plays an important role in the high-pressure behavior of these materials.[16] The cinnabar, NaCl, and Cmcm phases of HgSe and HgTe are all reported to be site ordered.[1] There is evidence of a post-Cmcm phase in HgTe at pressures above 28 GPa,[1,13] whereas for HgSe the Cmcm phase survives up to the highest pressures reached in experiments for this material of 50 GPa.[1]

Further emphasizing the similarities between the behavior of HgSe and HgTe, the zincblende phases of both compounds undergo similar orthorhombic distortions just above the onset of their respective transitions to the cinnabar phase, resulting in a structure with space group (SG) $C222_1$.[17,18] The zincblende → $C222_1$ transition in HgSe and HgTe is a "hidden" transition that occurs at ∼2 GPa, at which the sluggish zincblende → cinnabar transition has already begun but has not yet completed.[17] The $C222_1$ phases of both materials are metastable and coexist in a small pressure interval along with the cinnabar and untransformed zincblende phases, transforming, in turn, into the cinnabar phase as the pressure is further increased. So far, this $C222_1$ structure has not been experimentally observed in any other binary compound.

Despite the power of first-principles total-energy methods based on the density-functional theory (DFT) in studying high-pressure stability (see, for example, Ref. 16 and references therein), only a few such studies have been reported for mercury chalcogenides. In their early theoretical study of HgSe and HgTe using the linearized-augmented plane-wave (LAPW) method, Lu *et al.* considered only the NaCl structure and the binary analog of the β-Sn structure (b-β-Sn) as candidate high-pressure phases.[19] Sun and Dong have studied the cinnabar phase of HgS using the WIEN2K code (LAPW plus local orbitals).[20] Some of us recently published a detailed study of the zincblende → $C222_1$ transition in HgSe and HgTe using the plane-wave pseudopotential (PWPP) method,[18] and Hao *et al.*[21] have also used this method to calculate the energetics of several high-pressure phases in HgTe. In Ref. 18 we focused on the dynamical stability of the low-pressure zincblende phases of HgSe and HgTe and the zincblende → $C222_1$ transition, and examined in detail the metastable $C222_1$ phase. That study pertained to the region of moderate compressions (up to ∼2–3 GPa) slightly above the onset of stability of the first of the high-pressure phases displayed by these materials, viz., the cinnabar phase, and the stability of the cinnabar phase and the other higher-pressure phases experimentally observed were not discussed.[22] We were able to relate the occurrence of the $C222_1$ phases in HgSe and HgTe to a dynamical instability of the zincblende structures that, interestingly, are already very close to instability at rather low pressures.

In this paper we present the results of a comprehensive first-principles DFT study of the high-pressure phases of HgSe and HgTe, comprising the zincblende → cinnabar → NaCl → Cmcm sequence of transitions and including a study of the dynamical stability of the high-pressure cinnabar and NaCl phases. We thus complete a survey of the high-pressure stability of these compounds up to the interval of stability

of the highest-pressure phase that has been experimentally characterized, viz., the Cmcm phase. We will not discuss the post-Cmcm behavior of these materials.

The rest of this paper is organized as follows. The technical details of our first-principles DFT calculations are given in Sec. II. In Sec. III we provide a brief description of the structures considered. Section IV is devoted to presenting and discussing the results of our study, and we conclude with a summary of our main findings in Sec. V.

II. DESCRIPTION OF THE CALCULATIONS

The plane-wave DFT calculations were performed with the Vienna *ab initio* simulation package (VASP) (see Refs. 23 and 24 and references therein). We used the projector-augmented wave (PAW) scheme,[25,26] and the semicore 5*d* and the 6*s* electrons of Hg and the outermost *s* and *p* electrons of Se and Te were dealt with explicitly in the calculations. Basis sets including plane waves up to a kinetic-energy cutoff of 310 eV were used for both HgSe and HgTe in order to achieve highly converged results. Dense Monkhorst-Pack **k**-point grids were used for the Brillouin-zone integrations (e.g., a $20 \times 20 \times 20$ grid was used for the NaCl phases, and similar density grids were used for other metallic phases). The differences in total energy between phases were converged with respect to the basis set and **k**-point sets employed to within $\sim$1 meV per atom. We used both a local-density approximation (LDA) and generalized gradient approximation (GGA) exchange-correlation (XC) functionals. The Ceperley-Alder form (as parametrized by Perdew and Zunger)[27] was used for the LDA, and both the Perdew-Burke-Ernzerhof[28] (PBE) form and a more recent variant (PBEsol, Ref. 29) were used for the GGA. We remark that although there are significant quantitative differences between the results obtained with the different XC functionals, our results are qualitatively similar for each functional and support essentially the same picture of the high-pressure behavior of these compounds. We also checked the effects of spin-orbit corrections (SOC) on the stability of the phases, which could be *a priori* significant owing to the presence of the heavy element Hg in these compounds. However, we found the effects of SOC to be very small in both HgSe and HgTe, while their calculation substantially increased the computational expense. Although we will present results calculated including spin-orbit interaction to illustrate these effects, most of our results, unless otherwise stated, were obtained without SOC.

A review of the application of DFT-based total-energy methods to the study of the phase stability of semiconductors can be found in Ref. 16. In the present study we have focused on the pressure range up to the transition to the Cmcm phase, which is the highest-pressure phase properly characterized in experiments in HgSe and HgTe, and we have thus considered the observed high-pressure phases of these materials as well as several other candidate structures (see Sec. III). Our theoretical results are for hydrostatic conditions and zero temperature, and the small effects of zero-point motion have been neglected. Those phases with free structural parameters were fully relaxed at each volume through the calculation of the forces on the atoms and the stress tensor. The structural relaxation reduced the anisotropy in the diagonal components of the stress tensor to below 0.1 GPa and the forces on the atoms to below 0.005 eV Å^{-1}. We have found this level of accuracy to be sufficient to account for the main structural features of HgSe and HgTe under pressure.

To study the local dynamical stability, we have calculated the dynamical matrix for the relevant phases and their phonon spectra at different compressions within the quasiharmonic approximation through the calculation of the force-constant matrix using the method of finite displacements.[30–32] This method consists of calculating the forces on the atoms in a supercell geometry when small displacements from the equilibrium configuration are imposed on single atoms, from which an approximation to the force constants (and then the dynamical matrix) is obtained. Just three independent displacements (each in a different direction) per crystallographic orbit of symmetry-related atoms[33] are required, but point symmetry can reduce this number even further by relating displacements along different directions. A $4 \times 4 \times 4$ (128 atoms) supercell of the original fcc primitive cell (two atoms) was used for the NaCl structure and a $4 \times 4 \times 2$ supercell (192 atoms) was used for the cinnabar structure (six atoms in the primitive hexagonal cell), where two and six independent displacements are respectively required for the construction of the dynamical matrix. Displacements that preserve part of the symmetry of the equilibrium configuration can be constructed and by calculating forces for both small positive and negative deformations anharmonicities can be largely eliminated.[31] At special high-symmetry **k** points in the Brillouin zone (e.g., the zone-boundary *X* point of the NaCl structure), a more economical supercell, commensurate with wave vector **k** and thus able to represent exactly the pattern of atomic distortions of the phonons, was also used for calculating the pressure evolution of phonon frequencies.

III. CRYSTAL STRUCTURES

In this section we provide short descriptions and comments on the main structures considered in our calculations. Some of the structures are well known and a fuller description of them may be found in Refs. 1 and 16 and references therein, or in other standard texts.[34,35] Brief crystallographic descriptions of each of the binary structures considered in our study are given in Table I.

The most relevant structures are those of the phases that have stable intervals of pressure in these compounds, viz., the zincblende, cinnabar, rocksalt, and Cmcm structures. The $C222_1$ structure, which is an orthorhombic distortion of zincblende observed in HgSe and HgTe, was studied theoretically in Ref. 18. It will not be discussed further here, although we have included some data concerning this phase, for the sake of completeness. For a detailed account of the $C222_1$ structure, we refer the reader to the original paper of McMahon *et al.*, which reported observations of this structure in HgSe and HgTe,[17] and the descriptions in Refs. 1 and 18. (See also Fig. 1.)

At ambient conditions the stable phases of HgSe and HgTe adopt the fcc zincblende structure (hereafter abbreviated zb wherever appropriate). Zincblende has space group (SG) $F\bar{4}3m$, No. 216, and $Z = 4$ formula units per conventional unit cell, with cations at positions 4(*a*) (0,0,0) and anions at

TABLE I. Summary crystallographic descriptions of basic structures of the *AB* binary compounds considered. The positions of each atomic species *A* (cation) and *B* (anion) are indicated by giving the standard representative of each atomic orbit with respect to conventional axes, as well as its multiplicity and Wyckoff letter. Suffices *a* and *b* in the internal parameters stand for cation and anion, respectively.

Name	Space group	Atomic positions
Zincblende (zb)	$F\bar{4}3m$, No. 216	*A*: 4(*a*) (0, 0, 0) *B*: 4(*b*) (1/4, 1/4, 1/4)
$C222_1$	$C222_1$, No. 20	*A*: 4(*a*) (x_a, 0, 0) *B*: 4(*b*) (0, y_b, 1/4)
Cinnabar (cin)	$P3_121$, No. 152	*A*: 3(*a*) (x_a, 0, 1/3) *B*: 3(*b*) (x_b, 0, 5/6)
Tetrahedral cinnabar (cin-tet)	$P6_422$, No. 181	*A*: 3(*c*) (1/2, 0, 0) *B*: 3(*d*) (1/2, 0, 1/2)
NaCl	$Fm\bar{3}m$, No. 225	*A*: 4(*a*) (0, 0, 0) *B*: 4(*b*) (1/2, 1/2, 1/2)
Cmcm	*Cmcm*, No. 63	*A*: 4(*c*) (0, y_a, 1/4) *B*: 4(*c*) (0, y_b, 1/4)
Super-Cmcm (s-Cmcm)	*Cmcm*, No. 63	*A*: 4(*c*) (0, y_{a1}, 1/4) *A*: 8(*f*) (0, y_{a2}, z_a) *B*: 4(*c*) (0, y_{b1}, 1/4) *B*: 8(*f*) (0, y_{b2}, z_b)
CsCl	$Pm\bar{3}m$, No. 221	*A*: 4(*a*) (0, 0, 0) *B*: 4(*b*) (1/2, 1/2, 1/2)
b-β-Sn	$I\bar{4}m2$, No. 119	*A*: 2(*a*) (0, 0, 0) *B*: 2(*c*) (0, 1/2, 1/4)
Immm	*Immm*, No. 71	*A*: 2(*a*) (0, 0, 0) *B*: 2(*b*) (0, 1/2, 1/2)
NiAs	$P6_3mc$, No. 186	*A*: 2(*a*) (0, 0, $z_a = 0$) *B*: 2(*b*) (1/3, 2/3, $z_b = u$)
sc16	$Pa\bar{3}$, No. 205	*A*: 8(*c*) (x_a, x_a, x_a) *B*: 8(*c*) (x_b, x_b, x_b)
Wurtzite (wur)	$P6_3mc$, No. 186	*A*: 2(*b*) (1/3, 2/3, $z_a = 0$) *B*: 2(*b*) (1/3, 1/3, $z_b = u$)
HgO	*Pnma*, No. 62	*A*: 4(*c*) (x_a, 1/4, z_a) *B*: 4(*c*) (x_b, 1/4, z_b)

4(*c*) (1/4,1/4,1/4). In the zincblende structure each atom has ideal tetrahedral coordination (see Fig. 1).

The trigonal cinnabar-type structure (abbreviated cin) observed at moderately high pressures in HgSe and HgTe is the structure of the stable phase of HgS under ambient conditions (also referred to as α-HgS). It has SG $P3_121$, No. 152, and $Z = 3$, with cations at positions 3(*a*) (x_a,0,1/3) and anions at 3(*b*) (x_b,0,5/6).[36] Experimentally, $x(\mathrm{Hg}) = 0.662(1)$, $x(\mathrm{Se}) = 0.550(1)$, and $c/a = 2.320$ in HgSe at 4.0 GPa, 46.84 Å^3,[1] and $x(\mathrm{Hg}) = 0.641(1)$, $x(\mathrm{Se}) = 0.562(1)$, and $c/a = 2.287$ in HgTe at 3.6 GPa, 55.58 Å^3 (Ref. 9, see Fig. 2) [cf. the values for HgS under ambient conditions from Ref. 37, $x(\mathrm{Hg}) = 0.7196$, $x(\mathrm{S}) = 0.4919$, and $c/a = 2.288$]. These structural parameters result in $2 + 2 + 2$ coordination in HgSe and $4 + 2$ coordination in HgTe under moderately high pressure, quite unlike the $2 + 4$ coordination observed in HgS under ambient conditions.[1] This structure is sometimes described as being formed of spirals along the *c* axis composed of alternating cations and anions. The projected spirals of the cinnabar structure of HgTe are shown as solid lines in Fig. 2.

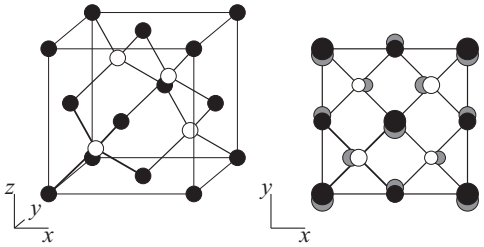

FIG. 1. The cubic zincblende structure is shown in perspective in a conventional crystallographic cubic cell on the left-hand side and in projection onto the *xy* plane on the right-hand side. The black and white circles indicate anion and cation positions, respectively. The gray circles in the projection represent atomic positions in the orthorhombic $C222_1$ structure, in which the atoms are displaced within the *xy* plane with respect to the zincblende structure.

The cubic NaCl structure [SG $Fm\bar{3}m$, No. 225, $Z = 4$, cations at 4(*a*) (0,0,0) and anions at 4(*b*) (1/2,1/2,1/2)] can be represented using the cinnabar description by taking $x_a = x_b = 2/3$ (or, equivalently, $x_a = x_b = 1/3$ and $c/a = \sqrt{6}$—see Figs. 2 and 3). (In this case the threefold cinnabar axis is directed along a body diagonal of the cubic NaCl cell.)

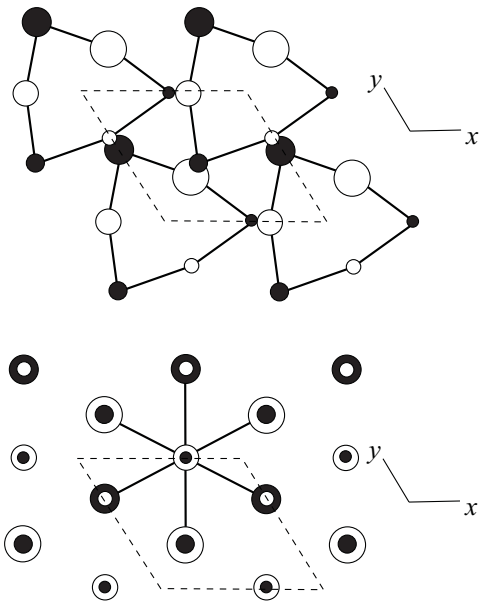

FIG. 2. (Top) The cinnabar structure of HgTe at ~3.6 GPa viewed along its threefold *c* axis, with the contour of the projected unit cell shown as a dashed line. The black and white circles represent anion and cation positions, respectively. Atomic planes of like atoms perpendicular to the main axis are separated by a distance of *c*/6. The differences in height are represented in the projected figure by different sized atoms. (Bottom) The rocksalt or NaCl structure, which can be considered as a special case of the cinnabar structure, plotted in a similar manner. In this case the *c* axis of the hexagonal cell in the cinnabar representation corresponds to the body diagonal of the cubic NaCl structure, which is also a threefold axis. Nearest-neighbor distances for the sixfold coordinated NaCl structure are shown by straight lines.

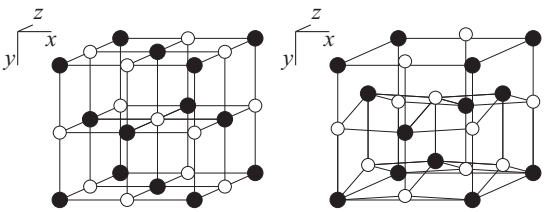

FIG. 3. The cubic NaCl structure (left-hand side) and orthorhombic Cmcm structure (right-hand side), shown in perspective. The black and white circles represent anion and cation positions, respectively. The Cmcm structure can be obtained from the NaCl structure by shearing alternate (001) planes in the [010] direction, which in turn results in puckering of the [100] atomic rows and an orthorhombic deformation of the cell.

Each atom in the NaCl structure is sixfold coordinated by atoms of the other species. The cubic CsCl structure [SG $Pm\bar{3}m$, No. 221, $Z = 1$, cations at 1(a) (0,0,0) and anions at 1(b) (1/2,1/2,1/2)] can also be represented by taking the same internal parameters as in NaCl and $c/a = \sqrt{6}/2$.[38] CsCl is eightfold coordinated. The CsCl structure has long been considered a candidate structure for the post-Cmcm phase of III–V and II–VI octet compounds on account of its low Madelung energy. Although we will not address this very-high-pressure regime here, we will show results for the CsCl phase as a reference and to provide an upper limit to stability.

Figure 3 shows the so-called Cmcm structure (named after its space group). This was described for the first time in ZnTe at high pressures (ZnTe-III, see Ref. 39) and has since turned out to occur commonly among the II–VI and III–V binary compounds under pressure.[1,16] It is orthorhombic, SG $Cmcm$ (No. 63, $Z = 4$) with cations at positions 4(c) $(0, y_a, 1/4)$ and anions at 4(c) $(0, y_b, 1/4)$, with $y_a - y_b$ not far from 0.5. Experimentally, in HgSe at 35.6 GPa, $y(\mathrm{Hg}) = 0.644$, $y(\mathrm{Se}) = 0.141$, $b/a = 1.079$, and $c/a = 0.965$ (see Ref. 15). [For HgTe at 18.5 GPa, $y(\mathrm{Hg}) = 0.624$, $y(\mathrm{Te}) = 0.152$, $b/a = 1.106$, and $c/a = 0.918$ (see Ref. 14).] The NaCl structure (of which Cmcm can be thought of as a distortion) corresponds to setting $y_a = 0.75$, $y_b = 0.25$ (or vice versa), and $b/a = c/a = 1$ in Cmcm. The Cmcm structure can be obtained from the NaCl structure by shearing alternate (001) planes in the [010] direction (Fig. 3).

The Cmcm structure can be viewed in yet another way as one of the simplest arrangements of two different atoms in a simple hexagonal lattice subject to the requirement of minimizing the number of like neighbors within the hexagonal planes.[40] Another such arrangement leads to the so-called Immm structure, which is closely related to the binary analog of the elemental β-Sn structure (here referred to as b-β-Sn). Both the tetragonal b-β-Sn and orthorhombic Immm structures can be represented in SG Imm2, No. 44 with cations in positions 2(a) (0,0,0) and anions in 2(b) (0,1/2,z), where $z = 1/4$ gives the b-β-Sn structure and $z = 1/2$ gives the Immm structure. The tetragonal b-β-Sn structure was once believed to occur in several high-pressure phases of octet binary compounds (and in particular HgSe-IV and HgTe-IV), but it was later ruled out in favor of the orthorhombic Cmcm structure.[1,15] The Immm structure has been observed in InSb under pressure.[41]

We also considered the NiAs-type structure, observed at high pressures in AlAs and AlP.[42] It consists of a stacking of hexagonal planes of alternating species, with atoms in one layer lying above the unoccupied centers of the adjacent layers.[43] The HgO-type structure is the orthorhombic structure of phase I of this material,[44] which is stable under normal conditions (although a cinnabar form is also observed).[45] The tetrahedral sc16 structure is the binary analog of the elemental bc8 structure obtained upon decompression of the β-Sn phase in Si and Ge.[46–48] It has been observed in GaAs as an intermediate high-pressure phase.[49,50] The hexagonal wurtzite structure (abbreviated wur) is that of the stable phases of the group-III nitrides and of ZnO, ZnS, CdS, and CdSe at ambient conditions.[1] For the ideal value of the axial ratio of $c/a = \sqrt{8/3}$ and internal parameter $u = 3/4$, the coordination is perfectly tetrahedral, as in zincblende but with a different relative orientation of adjacent tetrahedra.

Some other structures were also considered, such as the anti-NiAs structure (abbreviated a-NiAs), which results from interchanging the inequivalent sites of anions and cations in the NiAs structure, and the super-Cmcm structure observed in InSb (abbreviated s-Cmcm), which (as the "normal" Cmcm structure) corresponds to a distortion of the NaCl structure, involving in this case displacement of six (001) planes,[1] and the "tetrahedral" variant of the cinnabar structure (abbreviated cin-tet) observed in ZnTe-II.[51,52]

IV. RESULTS AND DISCUSSION

A. Energetics and relative stability of the structural phases

Figures 4 and 6 are representative of the results of our total-energy study. They show calculated energy-volume $E(V)$ curves of the structural phases investigated using the GGA-PBE functional without SOC, with energies given with respect

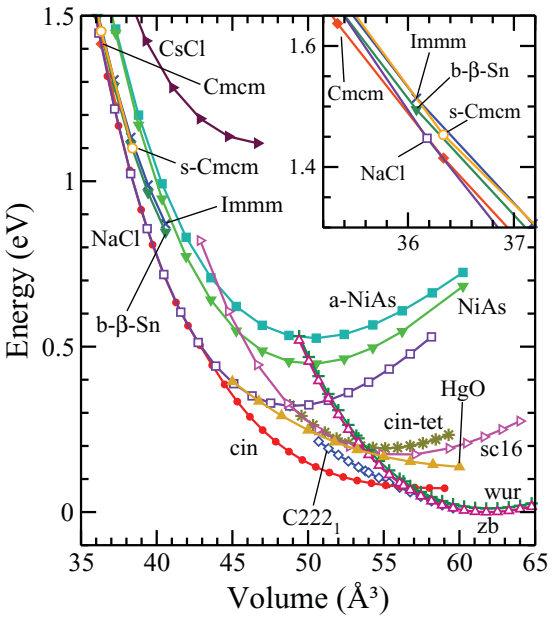

FIG. 4. (Color online) Energy-volume curves for the phases of HgSe calculated using the GGA-PBE. Both energies and volumes are given per formula unit. The energy is given with respect to that of the zero-pressure zincblende phase.

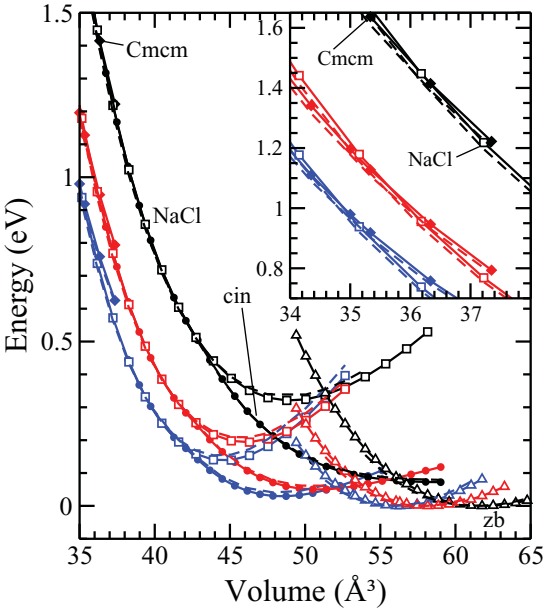

FIG. 5. (Color online) Comparison of the energy-volume curves for the observed phases of HgSe obtained using different XC functionals: (from left to right) LDA (blue), GGA-PBEsol (red), and GGA-PBE (black). Dashed curves correspond to data calculated including SOC, whereas solid curves and symbols correspond to data without SOC. In each case, the energy is given with respect to that of the zero-pressure zincblende phase.

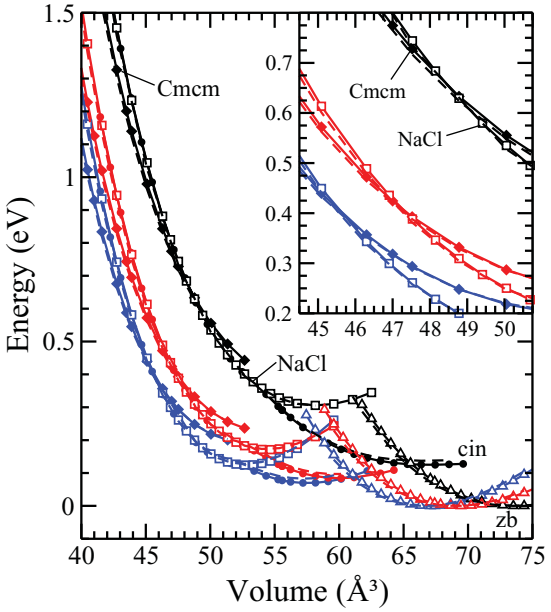

FIG. 7. (Color online) Comparison of the energy-volume curves for the observed phases of HgTe obtained using different XC functionals: (from left to right) LDA (blue), GGA-PBEsol (red), and GGA-PBE (black). Dashed curves correspond to data calculated including SOC, whereas solid curves and symbols correspond to data without SOC. In each case, the energy is given with respect to that of the zero-pressure zincblende phase.

to the zero-pressure zincblende phase.[53] [Hereafter all values of extensive quantities are given per formula unit (pfu).] In Figs. 5 and 7 we compare the $E(V)$ curves obtained using the different XC functionals for the observed zincblende, cinnabar, NaCl, and Cmcm phases. We remark that the calculated data obtained using each of the XC functionals are qualitatively similar. In Figs. 5 and 7 we also show our results for these phases obtained including spin-orbit interaction (dashed curves). The calculated spin-orbit effect is very small for each of the XC functionals considered, and in several cases the $E(V)$ curves with SOC and corresponding curves without SOC are hardly distinguishable on the scale used in the figures.

For each phase, the calculated $E(V)$ data were fitted, in appropriate volume intervals, using a fourth-order Birch-Murnaghan equation of state.[54] Figures 8 and 9 show pressure-volume $p(V)$ curves for the zincblende, cinnabar, NaCl, and

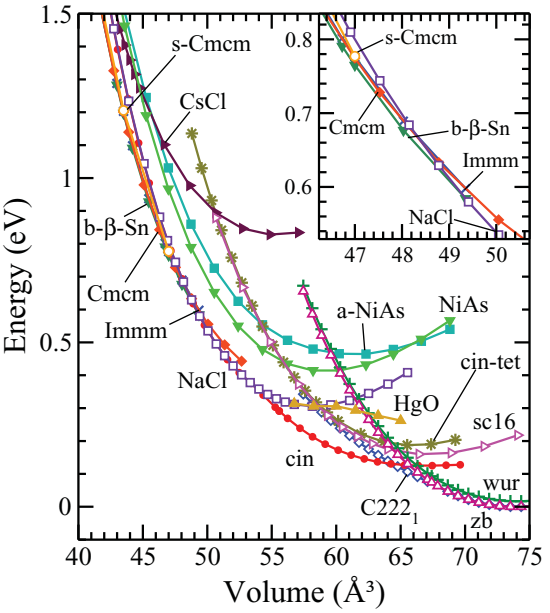

FIG. 6. (Color online) Energy-volume curves for the phases of HgTe calculated using the GGA-PBE. Both energies and volumes are given per formula unit. The energy is given with respect to that of the respective zero-pressure zincblende phases.

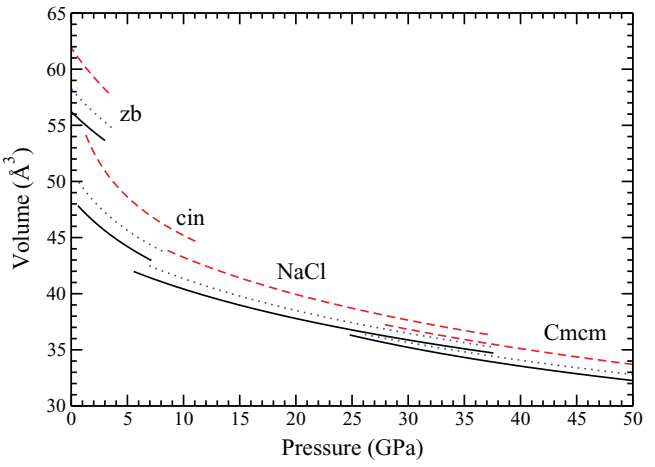

FIG. 8. (Color online) Calculated pressure-volume curves for the zincblende, cinnabar, NaCl, and Cmcm phases of HgSe, obtained using the LDA (black, solid curves), GGA-PBE (red, dashed), and GGA-PBEsol (blue, dotted) XC functionals.

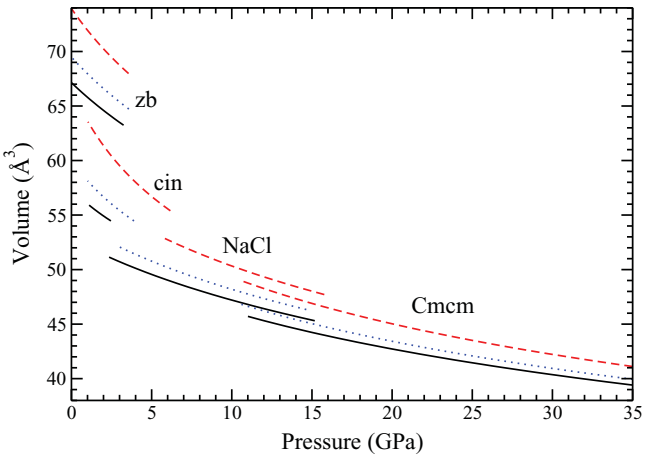

FIG. 9. (Color online) Calculated pressure-volume curves for the zincblende, cinnabar, NaCl, and Cmcm phases of HgTe, obtained using the LDA (black, solid curves), GGA-PBE (red, dashed), and GGA-PBEsol (blue, dotted) XC functionals.

Cmcm phases obtained from these fits, for the three different XC functionals. The enthalpy $H = E + pV$ was also obtained from the fits, and coexistence pressures between phases were calculated as the crossings of the $H(p)$ curves. [Alternatively, coexistence pressures can be inferred directly from the $E(V)$ plots through the common-tangent construction.[16]] Our calculated coexistence pressures for the observed high-pressure phases are given in Table III and compared with experimental values of the transition pressures.

Figures 4–7 correctly show the zincblende phases (phase I) of HgTe and HgSe to be stable at zero pressure, with cinnabar (phase II) slightly higher in energy and denser than zincblende. We remark upon the small calculated energy difference between the minima of the zincblende and cinnabar phases with the smallest values corresponding to the LDA and the somewhat larger values corresponding to the GGA-PBE, and that SOC slightly increase these energy differences by around 10 meV (see Table II). This is characteristic of the mercury compounds when compared to other members of the II–VI and III–V families. The cinnabar phase in HgS is still lower in energy with respect to zincblende and becomes the stable phase at zero pressure, while in HgO a low-energy metastable cinnabar phase has been observed under ambient conditions.[45]

TABLE II. Experimental (Ref. 56) and theoretical values (calculated using the LDA and GGA-PBE and GGA-PBEsol prescriptions; see the text) of the volume (in Å^3 per formula unit), bulk modulus (in GPa), and pressure derivative of the bulk modulus (dimensionless) of the zincblende phases of HgSe and HgTe at zero pressure. Theoretical values obtained with SOC are given in brackets. We also give the calculated difference in energy between the cinnabar and zincblende phases at zero pressure, $\Delta E_{\rm cin}$ (in meV).

zb-HgSe	V_0 (Å^3)	B_0 (GPa)	B_0'	$\Delta E_{\rm cin}$(meV)
Experiment	56.30	58	–	–
LDA	56.23 [55.83]	58 [59]	4.8 [4.8]	29 [40]
GGA-PBEsol	58.24 [57.80]	51 [52]	5.0 [5.1]	50 [61]
GGA-PBE	61.86 [61.39]	42 [43]	4.8 [4.8]	72 [79]
zb-HgTe	V_0 (Å^3)	B_0 (GPa)	B_0'	$\Delta E_{\rm cin}$(meV)
Experiment	67.43	48	–	–
LDA	67.03 [66.66]	47 [48]	4.9 [5.0]	70 [82]
GGA-PBEsol	69.41 [69.02]	42 [42]	4.9 [5.0]	84 [97]
GGA-PBE	73.95 [73.54]	34 [34]	5.0 [5.1]	125 [137]

The calculated equilibrium zero-pressure volume, bulk modulus, and pressure derivative of the bulk modulus of the ambient-pressure zincblende phases are collected in Table II, along with experimental data. We note that the values of these quantities calculated within the LDA are in excellent agreement with the experimental values for both HgSe and HgTe—a better agreement indeed than one has come to expect, where an underestimate of the equilibrium volume within the LDA is normally observed. On the other hand, the GGA tends normally to overestimate equilibrium volumes. Of the two GGA functionals used in our calculations, the more recent PBEsol variant yields equation-of-state parameters closer to experiment, whereas the PBE functional gives a larger overestimation of the equilibrium volumes and underestimation of the bulk moduli. We stress, however, that the qualitative picture of the high-pressure behavior of these compounds that emerges from the LDA and both GGA functionals is very similar. The main effect of SOC is seen to be to reduce slightly the value of the equilibrium zero-pressure volume.

As the pressure is increased, the zincblende phases of both HgSe and HgTe become thermodynamically unstable to the cinnabar structure (phase II). The small energy differences between the zincblende and cinnabar phases result in small values of the calculated zb/cin coexistence pressure p_c (see Table III), with the largest calculated values given by the GGA-PBE and the smallest by the LDA. The agreement between our calculated values of p_c(zb/cin) for all three XC functionals and the observed experimental transition pressures is remarkable. The zb→cin transition is of first order and the calculated relative volume reductions given in Table III are somewhat larger than the reported experimental values, with the largest deviation found for the LDA functional. The effect of SOC on the calculated coexistence pressures and volume reductions is very small, as it is also for the other higher-pressure transitions.

As the compression progresses, the $E(V)$ curves of the cinnabar phases, obtained with full relaxation of their structural degrees of freedom at each volume, merge continuously with the $E(V)$ curves of the NaCl phases (phase III). At the smaller volumes investigated for the cinnabar phases, their relaxation resulted in local minima that correspond to the NaCl structure, which can be considered a special configuration within the cinnabar representation (see Sec. III). We will comment in more detail on the structural aspects of the cin → NaCl transition in Sec. IV B. Note that there is a subtle change of curvature in the cinnabar $E(V)$ curves around the volumes at which they merge with the NaCl curves, and that a thermodynamical instability with respect to the NaCl phase occurs before the cinnabar phase has continuously evolved into NaCl, resulting in a weakly first-order transition with a small finite discontinuity in the volume and structural parameters, which is larger in HgTe than in HgSe. In other words, there is a common tangent between the $E(V)$ curves of the cinnabar and NaCl phases. The $p(V)$ curves represented in Figs. 8 and 9

TABLE III. Experimental values of the transition pressures, p_t, and our calculated coexistence pressures, p_c, (both in GPa) along with relative volume reductions (Ref. 57), ΔV (in percent), for the different transitions observed in HgSe and HgTe. The calculated coexistence pressures and volume reductions are given for the LDA, GGA-PBE, and GGA-PBEsol XC functionals. The values of these quantities calculated using SOC are given in brackets.

HgSe		Experiment	LDA	GGA-PBEsol	GGA-PBE
zb → cin	$p_{t/c}$	0.7,[a] 0.8,[b] 1.15[c]	0.6 [0.9]	1.1 [1.3]	1.9 [2.3]
	ΔV	9.0,[b] 9.9[c]	13.9 [13.7]	13.0 [13.0]	11.0 [10.8]
cin → NaCl	$p_{t/c}$	14.6,[c] 15.5[d,e]	7.0 [6.9]	9.0 [8.4]	11.5 [10.7]
	ΔV	0.2[c]	2.8 [3.0]	2.9 [2.6]	2.9 [3.0]
NaCl → Cmcm	$p_{t/c}$	28.0[f]	36.0 [34.0]	32.0 [32.0]	35.0 [36.0]
	ΔV	0.9[g]	1.4 [1.6]	1.3 [1.5]	1.3 [1.3]
HgTe		**Experiment**	**LDA**	**GGA-PBEsol**	**GGA-PBE**
zb → cin	$p_{t/c}$	1.3[a]	1.2 [1.4]	1.4 [1.7]	2.3 [2.6]
	ΔV	11[h]	14.5 [14.4]	14.3 [13.9]	12.2 [12.2]
cin → NaCl	$p_{t/c}$	8.0[d,e]	2.5 [2.0]	3.5 [3.0]	6.5 [5.6]
	ΔV	3[h]	5.2 [4.9]	4.5 [4.6]	3.9 [4.0]
NaCl → Cmcm	$p_{t/c}$	10.2[i]	12.5 [12.9]	11.0 [11.0]	12.5 [12.4]
	ΔV	1.2[i]	1.8 [1.7]	1.6 [1.6]	1.5 [1.5]

[a]Reference 2.
[b]Reference 5.
[c]Reference 17.
[d]Reference 6.
[e]Reference 7.
[f]Reference 11.
[g]Reference 15.
[h]Reference 10.
[i]Reference 14.

show the volume discontinuity associated with this transition. We note that the similarity of the diffraction patterns and the existence of microstructural effects in the diffraction profiles of the NaCl phase have made it difficult the experimental determination of the cin → NaCl volume change in HgSe.[1]

The relative stability of the cinnabar and NaCl phases and the nature of the cin → NaCl transition in HgSe and HgTe have also proven difficult to deal with in earlier theoretical work. Hao *et al.* were not able to evaluate the coexistence pressure of the cin and NaCl phases in their PWPP study owing to the alleged second-order character of the cin → NaCl transition[21] (however, their calculated zb/cin and NaCl/Cmcm coexistence pressures are in good agreement both with our own theoretical values and experimental values of the transition pressures). Within their study of the low-pressure zincblende phases of HgSe and HgTe, Cardona *et al.* provide also some complementary results pertaining high-pressure stability using the PWPP scheme.[55] Although their zb/cin coexistence pressures are in good agreement with experiments, they give far too large a value for the cin/NaCl coexistence pressure in HgSe (30 GPa) and no range of stability at all for the cinnabar phase in HgTe.

Our calculated cin/NaCl coexistence pressures turn out to be smaller than the experimental transition pressures, with the PBE values being the largest and closest to the experimental observations. In particular, we note that the LDA results for HgTe are too small and yield a reduced interval of stability for cin-HgTe. The reason for this is unknown to us. The NaCl structure can be represented within the cinnabar description using a nonprimitive hexagonal cell that is three times larger than the fcc primitive cell of NaCl and is oriented along its body diagonal (see Sec. III). Using this representation, a very accurate calculation of the energy difference between the NaCl and cinnabar phases can be performed. Our results for the NaCl phase calculated using a cinnabar-like representation agree perfectly with those using the normal description, although different sets of **k** points were used in each case, so we are satisfied with the numerical accuracy of our calculations and must attribute the discrepancy in the coexistence pressure to the use of the approximate LDA functional or to effects not taken into account in our study, for example, temperature. Our results are for zero temperature whereas most of the experimental data were taken at ambient temperature.

Upon further compression, the NaCl structure becomes thermodynamically unstable to the Cmcm structure (phase IV). At variance with observations in other III–V and II–VI compounds,[58] we find that the NaCl → Cmcm transition in HgSe and HgTe is first order, which agrees with the experimental data for these compounds.[1] The NaCl → Cmcm transition is discussed in detail in Sec. IV C. The much larger transition pressure for the NaCl → Cmcm transition in HgSe with respect to HgTe observed in experiments is correctly reproduced in our calculations. For HgTe we find good agreement between our calculated values of the NaCl/Cmcm coexistence pressure and the experimental values of the transition pressure (see Table III). However, the calculated NaCl/Cmcm coexistence pressure for HgSe is larger than the experimental transition pressure. The higher value of the

NaCl/Cmcm coexistence pressure in HgSe and the similar compressibilities of both phases at such pressure regime make the calculated values of the coexistence pressure in HgSe less accurate and more sensitive, in absolute terms, to effects neglected in our calculations. There are no experimental reports of the effect of temperature on the NaCl → Cmcm transition pressures for these materials, but our results indicate that such effects should be more pronounced in HgSe.

Interestingly, we find the energy curves of the b-β-Sn, Immm, and s-Cmcm structures to be rather close to that of the Cmcm structure in the pressure range in which Cmcm is observed. These phases can be considered as belonging to the same class or family of *pseudohexagonal* structures, corresponding to different orderings of two atomic species on a simple hexagonal lattice (with accompanying deformations introduced by the different decorations)[40] or small distortions of it (as in the case of the b-β-Sn structure), so their underlying geometry is similar. As can be seen in Figs. 4 and 6, they exhibit rather similar compressibilities in large pressure intervals, with small energy differences between them of the order of tens of meV. In our calculations for HgSe, in the relevant compression regime, the Cmcm structure is lower in energy within this pseudohexagonal family, with b-β-Sn lying next in energy by ∼10–20 meV and s-Cmcm and Immm somewhat higher. For HgTe we find that b-β-Sn is initially very slightly below Cmcm, with energy differences under ∼10 meV. The value of the NaCl/b-β-Sn coexistence pressure in this case is practically the same as that of the NaCl/Cmcm coexistence pressure. For all three XC functionals and for both materials, Immm is higher in energy than both Cmcm and b-β-Sn. Experimentally, a b-β-Sn-like structure was initially proposed [12,13] for what later was characterized as the Cmcm structure of both phases IV in HgSe and HgTe.[14,15] There is, however, an argument in favor of the NaCl → Cmcm transition. There is a simpler structural relationship between these two structures (see Secs. III and IV C) than between the NaCl and b-β-Sn structures, and the NaCl → Cmcm transition path may thus be preferred by nature. Indeed, the NaCl structure shows a tendency toward dynamical instability against the Cmcm distortion as pressure increases, and this becomes the favored phase as compression progresses (see Sec. IV C). Notwithstanding this, a b-β-Sn-like structure in HgTe cannot be ruled out by our calculations. We note also that in our calculations the b-β-Sn phase of HgTe appears to undergo a small orthorhombic distortion. The distorted structure has SG $C222_1$ with atomic positions 2(b) (1/2, 0.227, 3/4) (Hg) and 2(a) (0.249, 0, 0) (Te), and its cell is doubled with respect to that of b-β-Sn, with cell parameters $a = 1.4494$, $b = 0.5496$, and $c = 1.4496$ (at $p \sim 15$ GPa).

Let us comment briefly on the rest of the structural phases investigated, none of which comes close to stability in the relevant pressure interval of our study. The wurtzite phase is (approximately) uniformly higher in energy (by ∼11 meV in HgSe and ∼16 meV in HgTe) than the zincblende phase, to which it is structurally related, and has a very similar compressibility over the interval of pressures investigated. The calculated c/a ratios of wur-HgSe and wur-HgTe are ∼1.64, just slightly above the ideal value $\sqrt{8/3}$. The two tetrahedral sc16 and cin-tet phases also have rather similar $E(V)$ curves, and their zero-pressure equilibrium volumes are close to those of the respective cinnabar phases, but are somewhat higher in enthalpy and are not expected to occur as intermediate stable or metastable phases in these materials (as is, for example, observed in GaAs and ZnTe—see Ref. 1). The orthorhombic HgO-type structure evolves toward the NaCl structure at low pressures and is not a stable phase in any pressure range. The normal site-occupation NiAs structure is favored over the inverted site-occupation (anti-NiAs) at all positive pressures. At high pressures this NiAs phase undergoes a isostructural transition in which the c/a ratio abruptly increases from ∼1.8–1.9 to 3.2–3.9. This dramatic increase results in changes in coordination, with like nearest neighbors in the hexagonal planes being favored at such high compression. This modified NiAs structure, which is close in enthalpy to the CsCl structure, only occurs at rather high pressures and has not been represented in Figs. 4 and 6. The calculated Cmcm/CsCl coexistence pressure is ∼110 GPa in HgSe and 56 GPa in HgTe, which constitute upper bounds to the region of stability of the respective Cmcm phases.

B. The cinnabar phase and the cin → NaCl transition

The calculated structural parameters of the cinnabar phases are in excellent agreement with experiment. For example, in HgSe at a volume 47.0 Å^3 we find x(Hg) = 0.661, x(Se) = 0.569, and $c/a = 2.32$ using the LDA, in excellent agreement with the experimental values of x(Hg) = 0.662, y(Se) = 0.550, and $c/a = 2.320$ at this volume.[1] A similar level of agreement is obtained for HgTe [at the volume 55.6 Å^3, x(Hg) = 0.642, y(Te) = 0.561, and $c/a = 2.29$ (theory, LDA, this work); x(Hg) = 0.641, y(Te) = 0.562, $c/a = 2.287$ (experiment, Ref. 9)].

The structural transformation from the cinnabar to NaCl phase is easy to understand as the structures are simply related (see the description of NaCl in terms of the cinnabar structure in Sec. III). In the configuration space of the cinnabar structure, the NaCl structure is a special, higher-symmetry configuration which corresponds to taking the cinnabar internal parameters $x_a = x_b = 2/3$ and its axial ratio $c/a = \sqrt{6} \sim 2.449$. Our

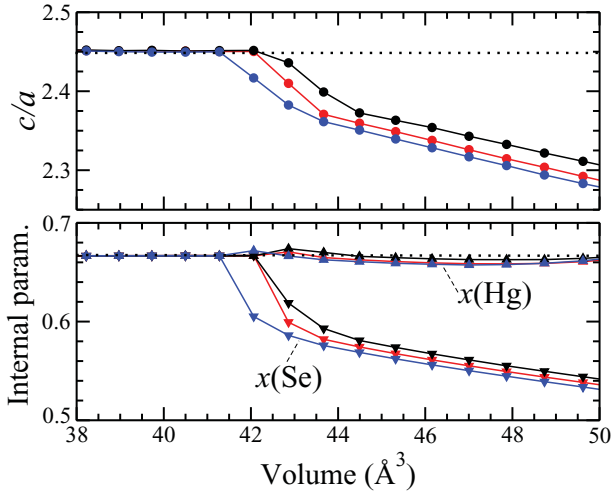

FIG. 10. (Color online) Evolution of the structural parameters of cin-HgSe under compression calculated using different XC functionals: LDA (blue), GGA-PBEsol (red), and GGA-PBE (black). The horizontal dotted lines give the values of the structural parameters corresponding to the NaCl structure (see Sec. III).

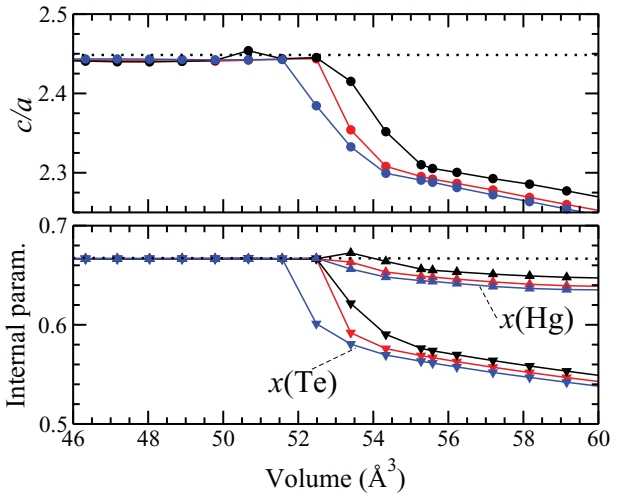

FIG. 11. (Color online) Evolution of the structural parameters of cin-HgTe under compression calculated using different XC functionals: LDA (blue), GGA-PBEsol (red), and GGA-PBE (black). The horizontal dotted lines give the values of the structural parameters corresponding to the NaCl structure (see Sec. III).

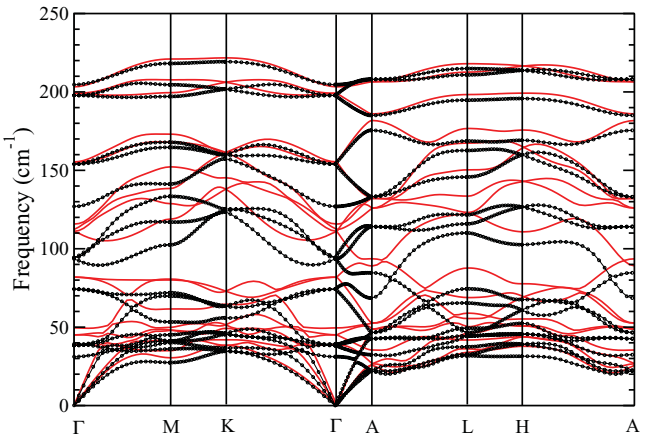

FIG. 12. (Color online) Calculated frequencies (within the GGA-PBE) of the vibrational modes $\omega(\mathbf{k})$ of cin-HgSe plotted along high-symmetry lines in the Brillouin zone, for $p = 3.8$ GPa (black circles) and $p = 7.7$ GPa (red lines). [$\mathbf{k}_\Gamma = 0$, $\mathbf{k}_M = (1/2,0,0)$, $\mathbf{k}_K = (1/3,1/3,1/3)$, $\mathbf{k}_A = (0,0,1/2)$, $\mathbf{k}_L = (1/2,0,1/2)$, $\mathbf{k}_H = (1/3,1/3,1/2)$ in terms of the conventional reciprocal generators of the hexagonal lattice.]

calculations for the structural relaxation of both compounds show an evolution of the cinnabar structure toward the NaCl structure with increasing pressure—see Figs. 10 and 11. Experiments cannot follow completely this evolution, because the transformation to NaCl takes place before,[10] and indeed we find that the cinnabar structure becomes thermodynamically unstable to NaCl before the evolution is completed. In both compounds, the internal parameter of the anion, x(Se) or x(Te), show a larger change under compression than the cation, x(Hg), which is in part related to their being farther from the special 2/3 NaCl value (which they both approach) than those of the cation and is in good agreement with the experimental observations.[10] The description of the structural evolution of the cinnabar phases given by our calculations essentially agrees with the experimental one reported for cin-HgTe in Ref. 10.

We have also investigated the effect of pressure on the phonon spectrum of the cinnabar phases of HgSe and HgTe. This is shown in Figs. 12 and 13, which give the calculated phonon frequencies of the phases at two different pressures. These phonon band structures were calculated using the PBE functional but similar results are obtained with the LDA and PBEsol. Upon compression and up to the calculated cin/NaCl coexistence pressure, the phonon-dispersion curves of the cinnabar phases are stable and show a general stiffening, which is more pronounced for the bands in the middle of the frequency spectrum. We note the existence of several low-energy bands (~25 cm^{-1} at zone-boundary points).

C. The NaCl → Cmcm transition and the Cmcm phase

The Cmcm structure can be obtained from the NaCl structure by shearing alternate (001) planes in the [010] direction (Fig. 3), a pattern of distortion that corresponds to a transverse-acoustic phonon at the X point $\mathbf{k}_X = (2\pi/a)(0,0,1)$, TA($X$), of the NaCl phase. This lowers the crystal symmetry (from cubic $Fm\bar{3}m$ to orthorhombic $Cmcm$), resulting in an orthorhombic deformation of the cell.[59] Several theoretical[16,50,60,61] and experimental[1,15] studies have shown that the NaCl structure becomes unstable under compression against this distortion in a number of III–V and II–VI compounds. This dynamical instability also occurs in HgSe and HgTe, although the NaCl → Cmcm transition shows several interesting peculiarities in these cases.

Our results confirm the experimental observation that the NaCl → Cmcm transition in HgSe and particularly in HgTe is distinctly first order.[14] This is different from the experimental and theoretical results for other members of the II–VI and III–V families[58] for which the observed NaCl → Cmcm transition seems to be second order or weakly first order at most.[1,16] The first-order character of the NaCl → Cmcm transition in HgSe and HgTe can be seen both in the calculated $E(V)$ curves of their NaCl and Cmcm phases (see the insets to Figs. 4–7) and in the calculated pressure evolutions of the

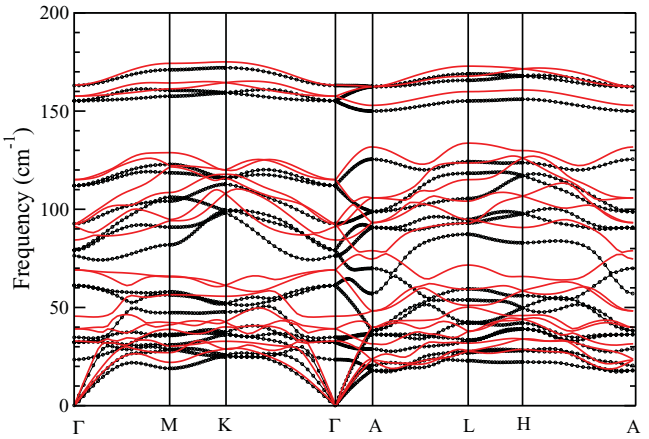

FIG. 13. (Color online) Calculated frequencies (within the GGA-PBE) of the vibrational modes $\omega(\mathbf{k})$ of cin-HgTe plotted along high-symmetry lines in the Brillouin zone, for $p = 2.4$ GPa (black circles) and $p = 5.6$ GPa (red lines).

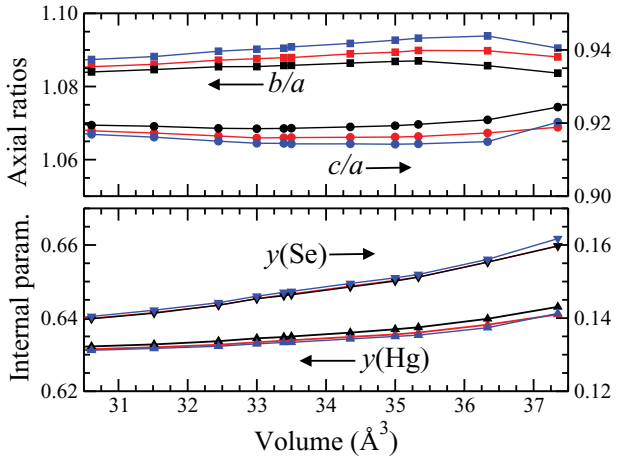

FIG. 14. (Color online) Evolution of the structural parameters of Cmcm-HgSe under compression calculated using different XC functionals: LDA (blue), GGA-PBEsol (red), and GGA-PBE (black).

structural parameters of the Cmcm phase shown in Figs. 14 and 15. In both HgSe and HgTe, the $E(V)$ curve of the Cmcm phase intersects that of the NaCl phase at a sharp angle, rather than merging smoothly as it would for a second-order or weakly first-order transition. This is more pronounced in the case of HgTe, where the first-order character of the transition is also stronger experimentally.[1] In keeping with this, the data for the structural parameters of Cmcm in Figs. 14 and 15 show that the Cmcm distortion is already well developed at the compressions at which the Cmcm phases are first observed. For example, using the LDA we find for Cmcm-HgTe the values $y(\mathrm{Hg}) = 0.623$, $y(\mathrm{Te}) = 0.153$, $b/a = 1.105$, and $c/a = 0.908$ at the volume 43.7 Å^3, in good agreement with the experimental values $y(\mathrm{Hg}) = 0.624$, $y(\mathrm{Te}) = 0.152$, $b/a = 1.106$, and $c/a = 0.918$ (Ref. 1) [cf. the values of the structural parameters corresponding to the NaCl structure of $y(\mathrm{Hg}) = 0.75$, $y(\mathrm{Te}) = 0.25$, $b/a = c/a = 1.0$.] For Cmcm-HgSe, $y(\mathrm{Hg}) = 0.635$, $y(\mathrm{Se}) = 0.152$, $b/a = 1.093$, and $c/a = 0.914$ at the volume 35.6 Å^3, cf. the

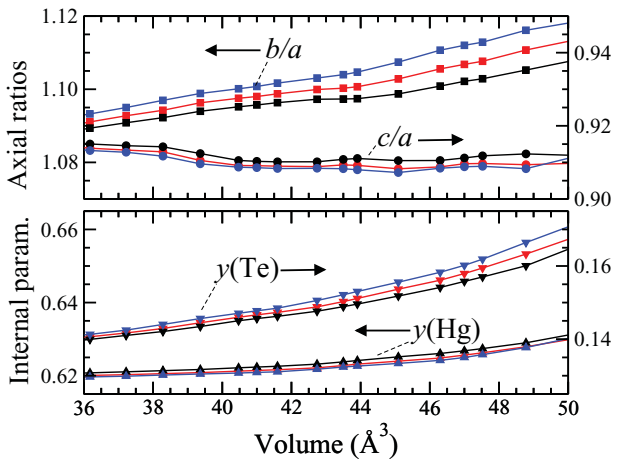

FIG. 15. (Color online) Evolution of the structural parameters of Cmcm-HgTe under compression calculated using different XC functionals: LDA (blue), GGA-PBEsol (red), and GGA-PBE (black).

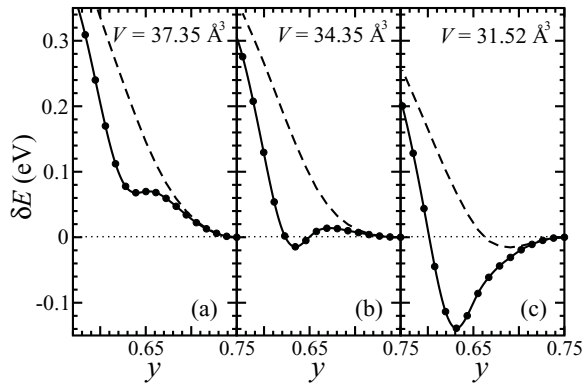

FIG. 16. Change in energy per formula unit of NaCl-HgSe along the path of its Cmcm distortion (see text). We use the value of the internal parameter y of the cation to indicate the position of the internal configuration along the path of distortion, with $y = 0.75$ representing the undistorted NaCl configuration (see Sec. III). At each of the three compressions depicted, the solid curve and the circles are for full relaxation of the cell shape at each point on the path of distortion, whereas the dashed curves correspond to keeping the shape fixed to that of the NaCl configuration.

experimental values $y(\mathrm{Hg}) = 0.644$, $y(\mathrm{Se}) = 0.141$, $b/a = 1.079$, and $c/a = 0.965$.[1]

In Figs. 16(a)–16(c) we show the change in energy (with respect to that of the NaCl structure) associated with the Cmcm distortion in HgSe, by plotting this change along the deformation path joining the NaCl structure [which corresponds to the point $(y_a, y_b) = (0.75, 0.25)$ in the configuration space of Cmcm (see Sec. III)] to the local minimum of the Cmcm structure. The direction of this path in (y_a, y_b) space corresponds approximately to that of the low-energy TA(X) eigenvector of the NaCl phase (which we will discuss later—see Figs. 17 and 18). The compression increases from Figs. 16(a) to 16(c). We have chosen to represent the change

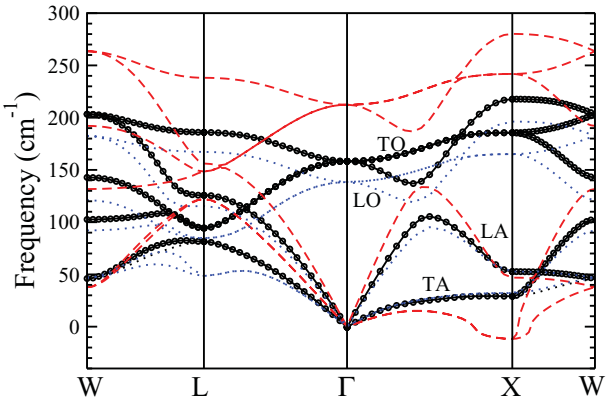

FIG. 17. (Color online) Calculated frequencies (within the GGA-PBE) of the vibrational modes $\omega(\mathbf{k})$ of NaCl-HgSe plotted along high-symmetry lines in the Brillouin zone at three different compressions. Full black lines and circles correspond to a pressure $p \sim 17.6$ GPa ($V = 40.47$ Å^3), red dashed lines correspond to a larger pressure of ~44.5 GPa ($V = 35.15$ Å^3), and blue dotted lines correspond to a smaller pressure of ~10.8 GPa ($V = 42.74$ Å^3). [$\mathbf{k}_\Gamma = 0$, $\mathbf{k}_X = (0,0,1)$, $\mathbf{k}_L = (1/2,1/2,1/2)$, $\mathbf{k}_W = (0,1/2,1)$, in units of $2\pi/a$.]

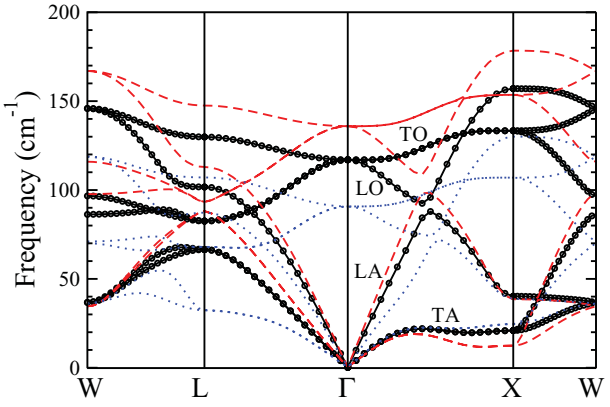

FIG. 18. (Color online) Calculated frequencies (within the GGA-PBE) of the vibrational modes $\omega(\mathbf{k})$ of NaCl-HgTe plotted along high-symmetry lines in the Brillouin at three different compressions. Full black lines and circles correspond to a pressure $p \sim 9.0$ GPa ($V = 50.69$ Å^3), red dashed lines correspond to a larger pressure of ~15.8 GPa ($V = 47.53$ Å^3) and blue dotted lines correspond to a smaller pressure of ~2.4 GPa ($V = 55.36$ Å^3).

in energy along the path against the y_a internal coordinate of the cation ($y_a = 0.75$ corresponds thus to the NaCl structure). The dashed lines represent the change in energy when keeping the shape of the cell fixed to that of the reference (cubic) NaCl configuration, with solid lines and symbols representing values obtained after full relaxation of the cell shape at each fixed point in configuration space.

At low enough compression [Fig. 16(a)] the NaCl structure is stable, but even at this stage another Cmcm local minimum has already developed. The early existence of this locally stable Cmcm state (which tends to become lower in energy than the NaCl state as the compression progresses) explains the experimental observation that, at the onset of the NaCl → Cmcm transition, the Cmcm distortion is already well developed. At somewhat higher pressure [Fig. 16(b)] the Cmcm minimum becomes lower than that of the NaCl structure, but the NaCl minimum, though very shallow, can still be discerned. As pressure further increases the NaCl structure finally becomes dynamically unstable against distortion along the deformation path considered in Figs. 16(a)–16(c). In Fig. 16(c) the NaCl minimum has already disappeared and only the Cmcm minimum remains, corresponding to the now stable Cmcm phase.

In turn, the Cmcm minimum eventually becomes unstable and disappears at low enough compressions. In our calculations, at the larger volumes of the Cmcm phases, the configuration resulting upon structural relaxation was NaCl. The Cmcm data shown in Figs. 4–7 for the largest volume correspond to the largest volumes at which the Cmcm phase energy minimum still exists.

We conclude from Fig. 16 that the cell relaxation is very important in the stabilization of the Cmcm phases of HgSe and HgTe, which is different from our earlier findings for the zb → $C222_1$ transition (see Ref. 18). Even before the onset of the instability in NaCl, cell relaxation is the main source of the Cmcm local energy minimum [see Fig. 16(a), solid curve] that, under compression, becomes the global minimum. In fact, before the dynamical instability of the NaCl phase has set in, internal displacements of atoms alone is *highly* energetically unfavorable—see Fig. 16(a), dashed curve. Once the onset of the instability of the NaCl configuration has been reached, cell relaxation accounts for most of the energy gain of the Cmcm configuration [cf. solid and dashed curves in Figs. 16(b) and 16(c)]. We conclude that the orthorhombic deformation of the cell is an important mechanism leading to the stabilization of the Cmcm phases in HgSe and HgTe and to the first-order character of their NaCl → Cmcm transition. This feature is unlike other members of the II–VI and III–V families,[58] for which the experimental NaCl → Cmcm transition is described as continuous, but it agrees with the experimental data for HgSe and HgTe.[1]

There is, however, softening upon compression of the TA branches in the Γ-X direction and eventually the TA(X) phonons become unstable. Figures 17 and 18 show calculated phonon frequencies along high-symmetry lines in the Brillouin zones of NaCl-HgSe and NaCl-HgTe at three different compressions. These curves display some interesting behavior. The optic bands stiffen (that is, shift upward in frequency) with increasing pressure approximately uniformly accross the Brillouin zone. The transverse-acoustic branches show, however, highly anisotropic, nonuniform behavior. For example, whereas in the Γ-X direction there is softening with pressure (negative Grüneisen parameter), in the Γ-L direction (or Λ points) these branches stiffen with pressure (positive Grüneisen parameter). Note that for the low-pressure zincblende phases of these compounds we had previously found that the TA branches soften with pressure irrespective of direction.[18] The behavior of the high-pressure NaCl phases is therefore quite unusual.

In Figs. 19 and 20 we show the pressure evolution of phonon frequencies of the NaCl phases calculated using the supercell method for the Γ and X points, as well as for the Λ point that corresponds to representing NaCl within the cinnabar description (that is, using an hexagonal supercell three times larger than its primitive fcc cell—see Sec. III). As mentioned before, the TA(X) instability is related to the NaCl → Cmcm transition on increase of pressure, whereas the softening of the

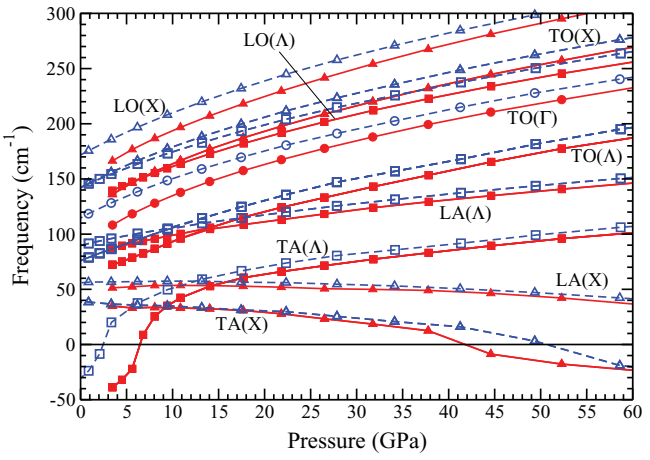

FIG. 19. (Color online) Calculated evolution with pressure of the phonon frequencies of NaCl-HgSe at the Γ (circles), X (triangles), and Λ (squares) points, calculated using the GGA-PBE (solid curves, filled symbols) and LDA (dashed curves, empty symbols).

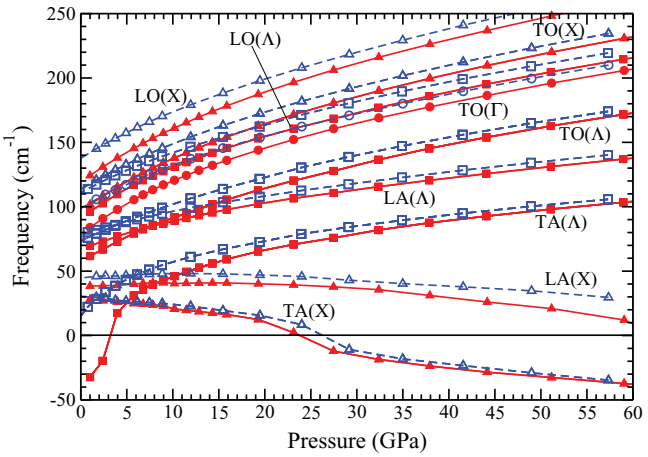

FIG. 20. (Color online) Calculated evolution with pressure of the phonon frequencies of NaCl-HgTe at the Γ (circles), X (triangles), and Λ (squares) points, calculated using the GGA-PBE (solid curves, filled symbols) and LDA (dashed curves, empty symbols).

TA(Λ) phonon upon decompression is related to the instability of the NaCl phase to cinnabar on decrease of pressure. The dynamical instability of the NaCl structure upon compression occurs, however, at pressures higher than the calculated onset of thermodynamical stability for the Cmcm phase. This is more pronounced in the case of HgTe for which the NaCl → Cmcm transition is experimentally more markedly first order.

Spin-orbit effects on the phonon frequencies at the Γ and X points were specifically checked and found to be small, within 4 cm^{-1} at most in both materials, and thus comparable to the numerical accuracy. For example, within the GGA-PBE, for HgSe at ∼17.6 GPa ($V = 40.47$ Å^3) the calculated TA(X) modes have a frequency of 29.7 cm^{-1} without SOC and 30.1 cm^{-1} with SOC. [For HgTe at ∼2.4 GPa ($V = 55.36$ Å^3) the TA(X) modes have a frequency of 25.8 cm^{-1} without SOC and 24.7 cm^{-1} with SOC.] SOC effects are significant for elemental Pb (atomic number $Z = 82$)[62] and Bi ($Z = 83$),[63] whose incomplete $6p$ shells are strongly affected by spin-orbit interaction,[62] but are very small for Pt ($Z = 78$) and Au ($Z = 79$),[64] which have an empty $6p$ shell, as does Hg ($Z = 80$).

V. CONCLUSIONS

In this work we have studied the structural behavior of HgSe and HgTe theoretically in the pressure range up to the observation of the so-called Cmcm phases, for which the existing body of experimental observations have asserted the nature of the different crystallograhic phases. We have used the PWPP method within the DFT formalism and have made a comparison of results obtained using the LDA, GGA-PBE, and GGA-PBEsol exchange-correlation functionals, as well as checking the effect of spin-orbit interaction on stability. We have studied the evolution of the phonon spectra of the cinnabar and NaCl phases and the dynamical stability of these high-pressure phases, and have thus provided a detailed analysis of the cin → NaCl and NaCl → Cmcm transitions.

The qualitative picture of the high-pressure behavior of these compounds that emerges from the LDA and both GGA functionals is very similar and in overall good agreement with experiment. Our results reproduce the sequence of phase transitions experimentally observed in these materials: zb → cin → NaCl → Cmcm. Our calculated coexistence pressures for the zincblende and cinnabar phases are of ∼1 GPa and are in remarkably good agreement with experiment. The effect of spin-orbit interaction on high-pressure stability was found to be very small.

The structural transformation from the cinnabar to NaCl phase is easy to understand as the two structures are simply related. Our calculations show an evolution of the cinnabar structure toward the NaCl structure with increasing pressure but the cinnabar structure becomes thermodynamically unstable to NaCl before the evolution is completed and there is a finite jump in the structural parameters and volume at the transition, which agrees with the experimental observations.[10] The phonon dispersion curves of the cinnabar phases show a general stiffening with increasing compression.

We have found that the orthorhombic distortion of the cubic cell is an important mechanism for energy gain in the NaCl → Cmcm transition that leads to the early stabilization of the Cmcm phase and, ultimately, to the discontinuous character of this transition in HgSe and HgTe. The mechanism accepted so far for the NaCl → Cmcm transition in II–VI and III–V binary compounds is the pressure-driven softening of the transverse-acoustic phonon branch in the Γ-X direction, leading to the eventual instability of the TA(X) phonons, whose pattern of distortion corresponds to that of the Cmcm phase. In HgSe and HgTe there is indeed softening of the TA(X) phonons, but although this softening is obviously related to the emergence of a Cmcm state as a global minimum state, the stabilization of the Cmcm phase takes place before the NaCl structure has become dynamically unstable. Experiments have shown the NaCl → Cmcm transition in other III–V and II–VI materials to be continuous, but in the case of HgSe and HgTe the Cmcm state is fully developed at the transition and the transition is, peculiarly, discontinuous and first order. On decrease of pressure from the Cmcm phase, the NaCl → Cmcm transformation should display some hysteresis, and a similar discontinuity in the evolution of the internal parameters of Cmcm as observed in the upstroke. Interestingly, the Grüneisen parameters of the TA branches of the NaCl phases are highly anisotropic and are positive in some directions within the Brillouin zone and negative in others.

In our calculations the pseudohexagonal geometries (Cmcm, s-Cmcm, and Immm) and the related b-β-Sn structure are rather close in energy. The b-β-Sn structure is in particular quite low in energy, which is interesting as some early experimental studies reported it as that of phase IV (Cmcm).[12,13] Though energetically close to Cmcm, the b-β-Sn-like structures have been ruled out by the most recent experimental studies,[1] which is in line with the combined phonon softening–orthorhombic deformation mechanism favoring the distortion of NaCl into Cmcm, which arises from our study.

ACKNOWLEDGMENTS

S.R., A.M., and J.L.S. acknowledge the financial support of the Ministerio de Educación of Spain through Grants No. MAT2007-65990-C03-03, No. MAT2010-21270-C04-03,

and No. CSD2007-00045. R.J.N. acknowledges the financial support of the Engineering and Physical Sciences Research Council (UK). Computing time at the Red Española de Supercomputación (Atlante supercomputer) is gratefully acknowledged. A.M. also thanks the Gobierno de Canarias for financial support through its research mobility program, and Pablo López Ríos for help in the final stages of preparing this article.

[1] R. J. Nelmes and M. I. McMahon, Semicond. Semimet. **54**, 145 (1998), and references therein.
[2] P. W. Bridgman, Proc. Amer. Acad. Sci. **74**, 21 (1940).
[3] J. A. Kafalas, H. C. Gatos, M. C. Levine, and M. D. Banus, J. Phys. Chem. Solids **23**, 1541 (1962).
[4] A. N. Mariano and E. P. Warekois, Science **142**, 672 (1963).
[5] A. Jayaraman, W. Klement Jr., and G. C. Kennedy, Phys. Rev. B **130**, 2277 (1963).
[6] A. Onodera, A. Ohtani, M. Motobayashi, T. Seike, O. Shimomura, and O. Fukunaga, in *Proceedings of the 8th AIRAPT Conference*, Uppsala, edited by C. M. Backman, T. Johannisson, and L. Tengner (World Scientific, Singapore, 1982), p. 321.
[7] A. Ohtani, T. Seike, M. Motobayashi, and A. Onodera, J. Phys. Chem. Solids **43**, 627 (1982).
[8] S. B. Qadri, A. W. Webb, E. F. Skelton, N. Moulton, J. Furdyna, and L. Colombo, High Press. Res. **4**, 303 (1990).
[9] N. G. Wright, M. I. McMahon, R. J. Nelmes, and A. San-Miguel, Phys. Rev. B **48**, 13111 (1993).
[10] A. San-Miguel, N. G. Wright, M. I. McMahon, and R. J. Nelmes, Phys. Rev. B **51**, 8731 (1995).
[11] T.-L. Huang and A. L. Ruoff, Phys. Rev. B **27**, 7811 (1983).
[12] A. Werner, H. D. Hochheimer, K. Strössner, and A. Jayaraman, Phys. Rev. B **28**, 3330 (1983).
[13] T.-L. Huang and A. L. Ruoff, Phys. Rev. B **31**, 5976 (1985).
[14] M. I. McMahon, N. G. Wright, D. R. Allan, and R. J. Nelmes, Phys. Rev. B **53**, 2163 (1996).
[15] R. J. Nelmes, M. I. McMahon, and S. A. Belmonte, Phys. Rev. Lett. **79**, 3668 (1997).
[16] A. Mujica, A. Rubio, A. Muñoz, and R. J. Needs, Rev. Mod. Phys. **75**, 863 (2003).
[17] M. I. McMahon, R. J. Nelmes, H. Liu, and S. A. Belmonte, Phys. Rev. Lett. **77**, 1781 (1996).
[18] S. Radescu, A. Mujica, and R. J. Needs, Phys. Rev. B **80**, 144110 (2009).
[19] Z. W. Lu, D. Singh, and H. Krakauer, Phys. Rev. B **39**, 10154 (1989).
[20] S.-R. Sun and Y.-H. Dong, Phys. Rev. B **72**, 174101 (2005).
[21] A. Hao, X. Yang, R. Yu, C. Gao, Y. Han, R. Liu, and Y. Tiang, J. Phys. Chem. Solids **70**, 433 (2009).
[22] Our LDA results for the cinnabar phase and the zincblende→cinnabar transition were mentioned briefly in Ref. 18, for the sake of giving a proper account of the stability limits of the zincblende phases.
[23] G. Kresse and J. Hafner, Phys. Rev. B **47**, 558 (1993).
[24] G. Kresse and J. Furthmüller, Comput. Mater. Sci. **6**, 15 (1996); Phys. Rev. B **54**, 11169 (1996). For more information see [http://cms.mpi.univie.ac.at/vasp].
[25] G. Kresse and D. Joubert, Phys. Rev. B **59**, 1758 (1999).
[26] Some calculations were also performed for testing purposes using ultrasoft pseudopotentials [D. Vanderbilt, Phys. Rev. B **41**, 7892 (1990)], finding good agreement with the PAW results.
[27] D. M. Ceperley and B. J. Alder, Phys. Rev. Lett. **45**, 566 (1980); as parametrized by J. P. Perdew and A. Zunger, Phys. Rev. B **23**, 5048 (1981).
[28] J. P. Perdew, K. Burke, and M. Ernzerhof, Phys. Rev. Lett. **77**, 3865 (1996).
[29] J. P. Perdew, A. Ruzsinszky, G. I. Csonka, O. A. Vydrov, G. E. Scuseria, L. A. Constantin, X. Zhou, and K. Burke, Phys. Rev. Lett. **100**, 136406 (2008).
[30] G. Kresse, J. Furthmüller, and J. Hafner, Europhys. Lett. **32**, 729 (1995).
[31] D. Alfè, Comput. Phys. Commun. **180**, 2622 (2009). Program available at [http://chianti.geol.ucl.ac.uk/∼dario].
[32] The supercell method does not, however, give a correct description of the optical bands around the Γ point (LO-TO splitting). This is irrelevant to the present study, which is mainly concerned with zone-boundary instabilities.
[33] That is, three independent displacements at most per orbit representative.
[34] R. W. G. Wyckoff, *Crystal Structures* (Interscience, New York, 1963).
[35] H. D. Megaw, *Crystal Structures: A Working Approach* (Saunders, Philadelphia, 1973).
[36] Although the $P3_121$ decription is normally adopted, the cinnabar structure can also be described in terms of the enantiomorphic SG $P3_221$, No. 154.
[37] T. Schleid, P. Lauxmann, and C. Schneck, Z. Kristallogr. Suppl. **16**, 95 (1999).
[38] The uniform uniaxial distortion from $c/a = \sqrt{6}$ to $c/a = \sqrt{6}/2$ in this description defines the so-called Bain transition path between the NaCl and CsCl structures.
[39] R. J. Nelmes, M. I. McMahon, N. G. Wright, and D. R. Allan, Phys. Rev. Lett. **73**, 1805 (1994).
[40] A. A. Kelsey and G. J. Ackland, J. Phys. Condens. Matter **12**, 7161 (2000).
[41] R. J. Nelmes, M. I. McMahon, P. D. Hatton, J. Crain, and R. O. Piltz, Phys. Rev. B **47**, 35 (1993); **48**, 9949(E) (1993).
[42] R. G. Greene, H. Luo, T. Li, and A. L. Ruoff, Phys. Rev. Lett. **72**, 2045 (1994).
[43] Although the NiAs-type structure is often referred to as having space group $P6_3mc$, the value of the internal parameter u in AlAs and AlP is 0.25, which increases the symmetry [SG $P6_3/mmc$, No. 194, 2(a) (0, 0, 0) (A), 2(c) (1/3, 2/3, 1/4) (B)].
[44] K. Aurivillius, Acta Crystallogr. **9**, 685 (1956); Acta Chem. Scand. **10**, 852 (1956).
[45] K. Aurivillius and I.-B. Carlsson, Acta Chem. Scand. **11**, 1069 (1957); **12**, 1297 (1958).
[46] J. S. Kasper and S. M. Richards, Acta Crystallogr. **17**, 752 (1964).
[47] A. Mujica and R. J. Needs, Phys. Rev. B **48**, 17010 (1993).
[48] R. J. Needs and A. Mujica, Phys. Rev. B **51**, 9652 (1995).
[49] M. I. McMahon, R. J. Nelmes, D. R. Allan, S. A. Belmonte, and T. Bovornratanaraks, Phys. Rev. Lett. **80**, 5564 (1998).

[50] A. Mujica, R. J. Needs, and A. Muñoz, Phys. Rev. B **52**, 8881 (1995).

[51] M. I. McMahon and R. J. Nelmes, Phys. Rev. Lett. **78**, 3697 (1997).

[52] A. Mujica, A. Muñoz, and R. J. Needs, Phys. Rev. B **57**, 1344 (1998).

[53] See supplementary material at [http://link.aps.org/supplemental/10.1103/PhysRevB.83.094107] for the energy-volume curves corresponding to the LDA and GGA-PBEsol XC functionals.

[54] F. Birch, Phys. Rev. **71**, 809 (1947).

[55] M. Cardona, R. K. Kremer, R. Lauck, G. Siegle, A. Muñoz, and A. H. Romero, Phys. Rev. B **80**, 195204 (2009).

[56] *Data in Science and Technology: Semiconductors Other Than Group IV Elements and III–V Compounds*, edited by O. Madelung (Springer, Berlin, 1992), and references therein.

[57] We note that different definitions of the relative volume reduction can be found in the literature. Here we use $\Delta V = (V^t_{\rm lp} - V^t_{\rm hp})/V_0$, where $V^t_{\rm lp}$ and $V^t_{\rm hp}$ are, respectively, the volumes of the low- and high-pressure phases involved in the transition at their experimental transition pressure (or calculated coexistence pressure) and V_0 is the zero-pressure equilibrium volume of the ambient-pressure zincblende phase.

[58] Namely, InP, InAs, ZnSe, CdS, CdSe, and CdTe (see Ref. 1). GaP, AlSb, and ZnTe do not have stable NaCl phases, but transform instead from their respective zincblende (GaP and AlSb) or cinnabar (ZnTe) phases into a well-developed Cmcm phase.

[59] There is also "puckering" of the [100] atomic rows within the (001) planes, but this is a small effect that does not significantly change the shape of the NaCl-like (001) planes. The primitive unit cell of Cmcm is doubled with respect to that of zincblende.

[60] V. Ozoliņš and A. Zunger, Phys. Rev. Lett. **82**, 767 (1999).

[61] A. Mujica and R. J. Needs, J. Phys. Condens. Matter **8**, L237 (1996).

[62] M. J. Verstraete, M. Torrent, F. Jollet, G. Zérah, and X. Gonze, Phys. Rev. B **78**, 045119 (2008).

[63] L. E. Díaz-Sánchez, A. H. Romero, and X. Gonze, Phys. Rev. B **76**, 104302 (2007).

[64] A. Dal Corso, Phys. Rev. B **76**, 054308 (2007).